The Pan-Arctic Catchment Database (ARCADE)

Niek Jesse Speetjens[1], Gustaf Hugelius[2], Thomas Gumbricht[2], Hugues Lantuit[3], Wouter R. Berghuijs[1], Philip A. Pika[1], Amanda Poste[4], Jorien E. Vonk[1]

[1]Vrije Universiteit Amsterdam (VUA), Department of Earth Sciences, Earth and Climate Cluster, Amsterdam, 1081 HV Amsterdam, The Netherlands
[2]Stockholm University (SU), Department of Physical Geography and Bolin Centre for Climate Research, 106 91 Stockholm, Sweden
[3]Alfred Wegener Institute (AWI) Helmholtz Centre for Polar and Marine Research, Ecological Chemistry Research Unit, 27570 Bremerhaven, Germany
[4] Norwegian Institute for Water Research (NIVA), Section for Nature based solutions and aquatic ecology, Økernveien 94, 0579 Oslo, Norway

Correspondence to: Niek Jesse Speetjens (n.j.speetjens@vu.nl/niek.j.speetjens@gmail.com)

Abstract

The Arctic is rapidly changing. Outside the Arctic, large-sample catchment databases have transformed catchment science from focusing on local case studies to more systematic studies of watershed functioning. Here we present an integrated pan-ARctic CAtchments summary DatabasE (ARCADE) of >40,000 catchments that drain into the Arctic Ocean and range in size from 1 km^2 to 3.1 x 10^6 km^2 (Speetjens et al., 2022). These watersheds, delineated at a 90-m resolution, are provided with 103 geospatial, environmental, climatic, and physiographic catchment properties. ARCADE is the first aggregated database of pan-Arctic river catchments that also includes numerous small watersheds at a high resolution. These small catchments are experiencing the greatest climatic warming while also storing large quantities of soil carbon in landscapes that are especially prone to degradation of permafrost (i.e., ice-wedge polygon terrain) and associated hydrological regime shifts. ARCADE is a key step toward monitoring the pan-Arctic across scales and is publicly available: https://dataverse.nl/dataset.xhtml?persistentId=doi:10.34894/U9HSPV.

1 Introduction

Earth's rapidly changing climate is particularly evident in the Arctic. Decreasing sea ice extent has amplified Arctic warming, which has led to an increase in mean land-surface air temperature of 3.1° C (three times the global average of ~1° C) over the period 1979 – 2019 (AMAP, 2021; GISTEMP Team, 2021). Under all IPCC climate scenarios, the Arctic will be substantially different by mid-century (e.g., less snow and sea ice, degraded permafrost, and altered ecosystems) (Overland et al., 2019). The Arctic

is important in regulating the global climate system (IPCC, 2019; IPCC, 2021) and global biogeochemical cycles (Parmentier et al., 2017). Ongoing changes in the Arctic and their consequential impacts are both local (e.g., ecosystem changes, changing food web interactions, and potential loss of biodiversity) (Vincent, 2019) and global (e.g., changing atmospheric circulation, ocean acidification, and an altered carbon cycle) (Box et al., 2019; Yamanouchi & Takata, 2020) which raises the urgency to understand this intricate system better.

In the Arctic, marine and terrestrial systems are tightly coupled. More than 10% of global river discharge flows into the Arctic Ocean (AO), which only contains about 1% of the global ocean volume (Aagaard and Carmack, 1989; McClelland et al., 2012). In addition, river discharge transports sediment, (organic) carbon, nutrients, and contaminants (Terhaar et al., 2021) into the AO. Arctic rivers integrate over local to regional scales and are therefore useful for studying the impacts of environmental and climatic change at various scales (Holmes et al., 2012).

Permanently frozen soils (permafrost) that are rich in organic carbon (OC) (Hugelius et al., 2014; Mishra et al., 2021) underlie about 60 - 80% of the AO watershed (Zhang et al., 2000; Obu et al., 2019). Permafrost conditions have long stabilized the subsurface, but ground temperatures are now warming across the northern hemisphere (Biskaborn et al., 2019). Permafrost degradation occurs slowly through deepening of the active layer (the layer that thaws during summer and refreezes during winter) (Ran et al., 2022) or more quickly through abrupt thaw of permafrost with high ground ice contents. Both types of thaw expose soil OC to degradation, which transforms it into greenhouse gases. Thus, the thawing of permafrost can accelerate global warming but also impacts hydrological, biogeochemical, and ecological processes in Arctic ecosystems, with complex consequences for lateral transport of terrestrial material to downstream freshwater and marine systems (Vonk & Gustafsson, 2013).

Investigations of Arctic change (e.g., Schuur et al., 2015; Walvoord & Kurylyk, 2016; Liljedahl et al., 2016; Lafrenière & Lamoureux, 2019; Bruhwiler et al, 2021) critically rely on data. The "Arctic Great Rivers Observatory" initiative, that runs since 2003, is a unique data set covering the six largest Arctic rivers (McClelland et al., 2008, www.arcticgreatrivers.org). While data on these large river systems can provide important insights into Arctic change (e.g., Wild et al., 2019; Terhaar et al., 2021; Behnke et al., 2021), they do not reveal the changes that occur at finer scales. Revealing such insights requires data from smaller Pan-Arctic watersheds.

Small and medium-sized watersheds drain roughly a third of the circumpolar landmass (Holmes et al., 2012). In contrast to the watersheds of the six largest Arctic rivers (Ob', Yenisey, Lena, Kolyma, Mackenzie, Yukon), the smaller watersheds are almost exclusively underlain by continuous permafrost (Holmes et al., 2012) and are often directly located at the coast. This makes these small watersheds fundamentally different from 'The Big Six' because large rivers drain to a few coastal locations (Mann et al., 2022), while the cumulative inputs of small watersheds are spread over a much larger coastal area. In addition, given their size and proximity to the AO, the changes in these watersheds could be more rapidly transferred and substantial to the Arctic coastal ecosystem.

75 Outside of the Arctic, the emergence of large-sample catchment databases (e.g., Hartmann et al., 2014; Newman et al., 2015; and Alvarez-Garreton et al., 2018), which combine data from many watersheds, have transformed the field from an emphasis on local case-studies towards more systematic insights into drivers of watershed functioning. For example, large-sample watershed studies allow to reveal regional differences (and similarities) in hydrological response, make space-for-time transformations, and

80 systematically test hypotheses. This has proven critical in, for example, understanding the impacts of climate change (e.g., Berghuijs et al., 2014) and testing modeling implications (e.g., Knoben et al., 2020). Such developments have not yet been possible in the Arctic, as large-sample databases of smaller watersheds are not yet available.

85 Here we present an integrated pan-ARctic CAtchments summary DatabasE (ARCADE) of >40,000 catchments, including small and medium-sized watersheds, draining into the Arctic Ocean. These watersheds, delineated at a high-resolution (90 m), are coupled with comprehensive information from various geospatial environmental, climatic, and physiographic datasets with pan-Arctic coverage. This publication aims to provide a high-resolution geographical register, relevant to those studying

90 environmental and climatic changes in relation to Arctic catchment hydrology and biogeochemistry.

2. Methods

2.1 Spatial extent and projection

The ARCADE database encompasses all major and minor drainage basins that are considered part of the pan-Arctic watershed, draining into the Arctic Ocean and surrounding seas. More specifically, this

95 includes all watersheds with a Strahler order of five (i.e. at least five hierarchical branching orders) or larger that drain into the Arctic Ocean as well as basins draining into the Bering Sea, and North of the Yukon River outlet with inclusion of the Yukon River. This follows the pan-Arctic watershed definition as defined by McGuire et al. (2009), with an area of 20.4×10^6 km^2, including the Canadian Archipelago, Greenland, and Hudson Bay (fig. 1). The data presented here have been transformed/re-projected to

100 WGS84 / NSIDC EASE-Grid 2.0 North (EPSG:6931) projection, an equal-area projection system designed for gridding and small-scale digital mapping for environmental sciences in the Northern Hemisphere (Brodzik et al., 2014).

2.2 Watershed delineation

2.2.1 Digital elevation model (DEM)

105 Terrain parameters such as altitude, slope, aspect, topographic position index, and Slope Length and Steepness factor (LS-factor) (Renard et al., 2017) were derived and calculated from Copernicus DEM GLO-90, a high-quality global 90-m resolution digital elevation model provided by the European Space Agency (ESA, 2021). The Copernicus DEM was accessed on 10 September 2021. For computational practicality, we chose the 90 m resolution product rather than the 30-m resolution product. The latter

110 could be used for future version updates of the ARCADE database. However, we deem the 90-m

resolution sufficiently detailed for our purposes (gaining insights in drainage areas on a pan-Arctic scale). We constrain the number of catchments in the database by using Strahler order 5 as the minimum outlet order and 1 km^2 catchment area as a lower threshold value (see next paragraph). A higher resolution DEM would not necessarily make for a better delineation. Moreover, most of the datasets used to link to the catchment areas have lower resolutions than 90 m. We are aware that, at any given resolution, the relative error regarding catchment delineation increases when looking at smaller watersheds. Yet, at our chosen resolution, we conclude there to be a reasonable tradeoff between efficiency and error.

2.2.2 Hydrological DEM conditioning and watershed extraction

The DEM was hydrologically conditioned (a.k.a. pit filling) before deriving flow direction, flow accumulation, Strahler order, watershed delineations, and topographic wetness index. This was done using the *r.hydrodem* module (Lindsay & Creed, 2005) in GRASS GIS (Neteler et al., 2012).

We delineated the watersheds at 90-meter resolution for subdivisions of the pan-Arctic landmass using the hydrologically-conditioned DEM. This subdivision was necessary because processing the DEM in one piece was computationally too intensive. Delineation was done using SAGA GIS (Conrad et al., 2015) using the module *Channel Network and Drainage Basins*. A lower threshold of Strahler order 5 was chosen to constrain watershed generation, i.e., only watersheds of streams with Strahler order 5 or higher at the outlet were delineated. This threshold was necessary to limit the number of watersheds in the final product and to ensure that only watersheds with actual streams were included. Another consideration was that as the watershed area approaches the DEM's source resolution, the relative accuracy decreases. Subdivisions of the pan-Arctic watersheds were combined into one dataset of all watersheds that drain into the AO (i.e., upstream areas of outlets at the AO). A known limitation of DEM-derived watershed delineation is that the algorithm struggles to find the channels and ridges in flat terrain. Since we are mostly interested in the drainage area, rather than channel location, errors in channels were tolerated more than errors in catchment boundaries. Small flat catchments (area < ~10 km^2 and slope < ~0.1° and mainly in fluvial deltas) are most prone to error, which is why we advise users to be critical when using these delineations for local purposes. Another limitation and source of uncertainty lies with watershed delineation on the Greenlandic icesheet. Here we simply proceeded delineating catchments using the surface/ice-topography as captured in the DEM.

2.3 Environmental data

All variables are described in supplementary table S1. Elaborated explanations are provided below.

2.3.1 Climatological data

Climatological data were extracted from the ERA5-Land Monthly Averaged – ECMWF Climate Reanalysis dataset (Muñoz-Sabater et al., 2019) using Google Earth Engine ("Planetary-scale geospatial analysis for everyone") (Gorelick et al., 2017). This dataset has a spatial resolution of 11,132 meters and consists of 50 bands containing climatological variables related to temperature, precipitation, evaporation, heat fluxes, wind, and vegetation. Minimum, maximum, mean, standard deviation, and median annual

values of a subset of these variables (a complete overview of all variables is available in S1) were calculated for each watershed from 01-01-1990 to 31-12-2019. In the case of pixels falling partly within the geometry of a watershed, the value is weighted by the fraction of each pixel that falls within the geometry. Precipitation, evaporation, and runoff totals were accumulated and averaged over the 30-year period (i.e., the mean annual total of each of these variables was calculated). For snow statistics, we calculated the 30-year average maximum snow depth (m), snow cover (%), snowmelt (m d^{-1}), and snowfall (m d^{-1}) based on the month with the highest value of each year. In the case of snowmelt, this is an indicator of the intensity of snowmelt during the melting season.

We also tested for trends using Sen's slope estimator for the same period. Sen (1968) calculates the slope as:

$$Q_i = \frac{(x_j - x_i)}{j - i}, i = 1,2,3, \dots, N \qquad (1)$$

Where x_j and x_i are records at time j and i ($j > i$). With n data records in a time series, the number of slope estimates equals $N = n(n-1)/2$. Q_i then follows by calculating the median of all the slope estimators. We chose to calculate these statistics on monthly data for temperature variables, while for snow-related variables, we only selected the winter months (November – April) and for evaporation-related variables only the summer months (June – September).

2.3.2 Physiographic data

Catchment properties

Basic catchment properties include minimum, maximum, mean, standard deviation and median of elevation (meters), slope (degrees), and aspect (degrees). Furthermore, we included centroid latitude (degrees), Gravelius index (watershed perimeter divided by the perimeter of a circle that has the same area; unitless), watershed perimeter (kilometers) and watershed area (square kilometers).

Soil properties

SoilGrids is a globally consistent dataset that contains soil properties (soil organic carbon (SOC) content (dg kg^{-1}), organic carbon density (dg dm^{-3}), nitrogen content (cg kg^{-1}), coarse fragments volumetric content (per 10,000), sand, silt and clay content (g kg^{-1}), soil bulk density (cg cm^{-3}) for six depth intervals (0-5 cm, 5-15 cm, 15-30 cm, 40-60 cm, 60-100 cm, 100-200cm), and organic carbon stock (OCS) (t ha^{-1}) for the upper 30 cm of the soil) and classes (the most the likely soil class according to the World Reference Base (WRB) classification system (IUSS Working Group WRB, 2014)) at 250-meter resolution (Poggio et al., 2021). The ARCADE database aggregates soil property data from SoilGrids into watershed minimum, maximum, mean and standard deviation. OCS was also summarized into total watershed OCS (Gt) in the upper 30 cm of the soil. Soil class data from SoilGrids were summarized by calculating the fractional coverage of each class for each watershed. All watershed statistics were calculated using the "image.reduceRegion()" function in Google Earth Engine (Gorelick et al., 2017). We

Deleted: monthly

Deleted: (i.e.,

Deleted:)

Formatted: Font: Not Bold

Deleted: As an example: A given watershed can have an average snowmelt of 0.021 m d^{-1}. This means that on average the month with the most snowmelt has an average snowmelt rate of 0.021 m d^{-1}, which can be seen as an indicator of intensity of the melting season

note that estimates of soil properties, especially for deeper soils, are often uncertain due to data scarcity in the permafrost region. We refer to Poggio et al., 2021 for more detailed discussions of uncertainties in the soil property projections.

Landcover class fractional cover

Watershed land cover fractional coverage was obtained from ESA WorldCover 10m v100 (Zanaga et al., 2021). This classifies the land surface at 10-meter resolution into 11 classes: trees, shrubland, grassland, cropland, built-up areas, barren/sparse vegetation, snow and ice, open water, herbaceous wetland, mangroves, moss and lichen.

Landform class fractional coverage

Another useful characterization parameter for watersheds is the fractional coverage of landforms. We chose to use a landform classification scheme proposed by Theobald et al. (2015). Their classification scheme maps ecologically relevant landforms (see supplementary tables included in dataset S1), which we deem of particular interest in characterizing a catchment, for instance to indicate sensitivity to the occurrence of abrupt permafrost thaw.

Burned area fraction coverage

Burned area fraction for each watershed over the period 2012 - 2022 was calculated from MODIS FireCCI5, a monthly global 250-meter spatial resolution burn scar classification product (Chuvieco et al., 2018). We selected and summarized recent (<10 yr) annual fire scars as they are most likely to have an ongoing and lasting effect on watershed biogeochemistry.

Permafrost extent

Permafrost fraction pixel cover was taken from the permafrost extent by Obu et al. (2019) and converted into watershed area fractional coverage per permafrost coverage type. The used product has a spatial resolution of 1 kilometer and a temporal range from 2000 – 2016. Continuous permafrost is classified as a pixel area coverage of 90-100%, discontinuous permafrost as 50-90%, sporadic permafrost as 10-50%, and isolated patches of permafrost as 0-10%.

Active layer thickness

Recently published high-resolution estimates of active layer thickness (ALT) (Ran et al., 2021) were summarized for each watershed. The source dataset has a 1-kilometer resolution for the period of 2000-2016. The authors generated the data by combining large amounts of field data combined with multisource geospatial remote sensing data into a statistical learning model. It has bias = 2.71 ± 16.46 cm and RMSE = 86.93 ± 19.61 cm for ALT.

Glacial fractional coverage

Glacial coverage was calculated by combining two datasets: Global Land Ice Measurements from Space (GLIMS) from which we used the latest available snapshot as of September 14, 2021, for the glacial extent (Kargel et al., 2014) and the Greenland Ice & Ocean Mask from the Greenland Mapping Project (GIMP) which contains a 15-meter resolution land ice mask for the Greenland ice sheet (Howat et al., 2014). We resampled the combined datasets to a 250-meter resolution grid to calculate fraction glacial coverage for each watershed.

Surface water fractional coverage

A high-resolution water mask, JRC Global Surface Water Mapping Layers, v1.3, (30 meter) (Pekel et al., 2016) was used to calculate fractional watershed area coverage. The conditions for the presence of water were determined by the occurrence of water in each cell for at least 50% of the time between 1984 and 2020.

Vegetation index

The summarized statistics of the normalized difference vegetation index (NDVI) and the Sen slope of NDVI were calculated using MOD13A1.006 Terra Vegetation Indices 16-Day Global 500m (Didan, 2015; accessed: 1 April 2022). This dataset is MODIS derived and has a 500-meter resolution. We used the annual maximum NDVI of each year from 2000 to 2021.

Topographic wetness index

As an indicator of terrain wetness, we used SAGA wetness index (Böhner & Selige, 2006), a modified topographic wetness index that is based on Moore et. al (1993). The indicator uses topography to differentiate catchments dominated by wetland terrain versus more well-drained terrain.

LS-factor

Slope Length and Steepness factor (LS-factor) is a factor used in the Universal Soil Loss Equation (USLE) (Renard et al., 2017) that serves as a predictor of soil loss ratio as a function of slope length and steepness. The LS-factor was calculated using SAGA GIS tool Module LS-factor which uses specific catchment area (SCA) as a substitute of slope length (Böhner & Selige, 2006).

Tasseled-cap trend index of visible spectra

As an indicator for changes in wetness (TCW), greenness (TCG) and brightness (TCB) (indicative of bare soil) we included tasseled cap indices derived from Landsat visible spectra images as provided by Nitze et al. (2018). The minima, maxima, and average of these pixel-based slopes were calculated for each watershed.

Moved down [1]: We used the annual maximum NDVI of each year from 2000 to 2021.

Moved (insertion) [1]

3. Results and discussion

3.1 Database inventory

285 The database consists of 47,054 watersheds ranging in size from 1 km^2 to 3.1 x 10^6 km^2 (Ob' watershed). We will refer to four groups of watersheds based on size (fig. 1, tables 1-5) because our work focuses on inventorying watersheds of all sizes and highlights the contrasts between the larger well-studied rivers and smaller rivers. The first group consists of 'The Big Six' (Ob', Yenisey, Lena, Mackenzie, Yukon, Lena Rivers) and one major watershed draining into the Hudson Bay (Nelson River). Therefore, the 'The
290 Big Six' becomes 'The Big Seven', abbreviated as BS. Then, 'The Middle Nine' (MN) consists of the Severnaya Dvina, Indigirka, Pechora, Olenek, Thelon, Yana, Khatanga, Pyasina and Taz Rivers. We then split the remaining watersheds into areas greater than 1000 km^2 (yet smaller than the MN), which we named "The Pan-Arctic 1000's" (PAT), and watersheds smaller than 1000 km^2, which we named the "The Pan-Arctic Small watersheds" (PAS).

295

The BS account for 50% of the total AO watershed area, while watersheds under 1000 km^2 (PAS) account for only 9% of the entire area. However, these small watersheds are much more abundant, and their landmass is more directly connected to the Arctic Ocean than the BS. Since large parts of the BS watersheds reach into low latitudes (~60% of their watershed areas are located south of 60° North, or
300 93% south of the Arctic Circle), the mean annual air temperature in these watersheds is higher compared to the rest of the pan-Arctic watershed (table 3), influencing mean permafrost coverage, active layer thickness (ALT), and occurrence of ice-wedge polygon terrain (table 4, 5, 6). These permafrost-related watershed properties are susceptible to change under climate warming trends and play a central role in Arctic watershed hydrology. Our database shows that the MN, PAT, and PAS watersheds have been
305 warming much faster than the BS (table 7), highlighting the need for more research on these smaller northern watersheds.

3.2 Data coverage

The hydrological functioning of small catchments in the Arctic remains uncertain. Therefore, our database provides a set of catchment properties to help address these uncertainties. Basic topographical catchment
310 metrics such as area, elevation, catchment slope, mean aspect, LS-factor, and TWI are available for all recorded catchments. Due to their resolution and extent, some of the other aggregated datasets have lower coverage. Most notably, ERA5-Land data has ~87% spatial coverage in the database. Most omitted watersheds are small coastal watersheds that were less than 50% covered by a cell of the ERA5-Land dataset. The same holds for the ALT and SoilGrids data which cover about ~82% and ~92% of all
315 watersheds, respectively. For all aggregated data sources, >80% of watersheds are covered.

3.3 Data quality assessment and limitations

The ARCADE database is the first published 90-meter resolution dataset of watersheds draining into the Arctic Ocean. A few unavoidable errors occurred during the watershed delineation. Errors most commonly arise in flat terrain where flow-routing algorithms struggle to determine the flow direction,

which troubles the watershed border definition. To deal with this, we used an internal SAGA function to artificially maintain a minimal channel slope by slightly altering the DEM. This minimal slope function effect is visually detectable in small deltas and floodplains where watershed borders sometimes appear less accurate than in steep, well-defined terrain. Additionally, this flow path uncertainty in flat terrain caused some errors in approximating the locations of coastal outlets. Given the high DEM resolution, these errors are generally in the order of meters rather than kilometers. This could be improved in future versions by 'burning' outlets and channels, for example derived from satellite imagery, into the DEM.

Our cut-off value in defining a river catchment (outlet Strahler order 5; minimum area of 1 km^2) leads to the omission of areas that lie within the pan-Arctic drainage basin but are outside our database's scope (i.e. so called wolf-tooth patches, remaining coastal areas in between catchments). However, we estimate the summarized area to be less than 1% of the total pan-Arctic watershed area. The strength of this database lies in the large spatial extent, its novelty and the range of spatially-explicit variables coupled to the delineated catchments. We therefore advise using this database to target specific (groups of) catchments and making comparisons among those to gain insight into spatial patterns, and localization of target areas for further research.

3.4 Pan-Arctic watersheds properties

ARCADE provides 103 variables with catchment properties divided over 353 columns (including statistics), showcasing a wide variability as well as spatial resemblances of catchments in the pan-Arctic drainage basin. Additionally, we provide summaries of the most important properties for the BS, MN, PAT, and PAS, both as a whole and on a regional basis (i.e., North America, Greenland, and Eurasia).

Physiographic features

Basic catchment-scale topographical information can be used to categorize watershed types and estimate their runoff, sediment transport regimes, and biogeochemical constituents. As an example, Connoly et al. (2018) found strong negative correlations between catchment slope and DOM and NO_3- concentrations in Arctic watersheds. According to the data presented here, PAS watersheds have on average the highest mean catchment slope. This is partially because Greenlandic small coastal watersheds are mountainous (table 3 and table 4). Eurasia and North America's proportion of PAT, on the other hand, consist of relatively low elevation, flat terrain (mean slope Eurasia: ~3.1 ±1.54°, North America: ~2.4 ±1.53°). The PAS watersheds are underlain mainly by continuous permafrost and feature wetland-type landcover (Eurasia: ~27% wetland North America: ~14% wetland) as opposed to BS (Eurasia 4% wetland, North America 1% wetland), with a high area-fraction of surface water (Eurasia: ~6% water, North America: ~8% water). Because of their permafrost coverage (mostly continuous), PAS watersheds are more likely to feature IWP terrain (37% IWP terrain in PAS as opposed to 1% IWP terrain in BS). Another noteworthy property of PAS watersheds is that, on average, they feature higher OC stocks (Eurasia: ~88 t ha^{-1}, Greenland: ~87 t ha^{-1}, North America: ~71 t ha^{-1}) than more commonly studied catchments (BS: ~64.5 t ha^{-1}, MN: ~69.5 t ha^{-1}). Additionally, Greenland stands out in most aspects, with a relatively high mean catchment slope (~7.5°), elevation (532 m amsl), and glacial coverage (77%) (table 4 and table 5). This

360 distinction in basic characteristics most likely distinguishes the lateral flux characteristics of Greenlandic watersheds from the rest of PAS. Greenland also includes several (149 out of 929) PAT catchments which are largely (>80% of their area) covered by the Greenlandic Ice Sheet. Since principles of watershed hydrology do not apply to ice sheets or glaciers, we advise users of this database to take note of the presence of these 'ice sheet watersheds' in the database. A solution to circumvent these watersheds is

365 filtering by fraction ice coverage to a value aligned with the study goals.

Climatological properties

Since MN, PAT and PAS are on average located in higher latitudes, these watersheds are colder than the BS (BS: -2.9 °C, MN: -10.5 °C, PAT: -9.1 °C, PAS: -10.4 °C) (table 3). While for the BS, the Eurasian watersheds are the coldest, the opposite is true for PAS (PAS of Eurasia: -4.7° C, North America: -11.0°

370 C. This is partially because the Gulf Stream warms smaller coastal watersheds of western Eurasia, but there might also already be some effect of temperature increase which has been greatest in the Eurasian PAS (+3.4° C; table 7). Annual precipitation, mean annual runoff, and the mean increase in precipitation over the past 30 years are highest in PAS and PAT (i.e., smaller watersheds) (table 7).

375 **Pan-Arctic trends in data**

We provide this database as a basis to explore the vast number of watersheds outside the BS and MN that have previously been lumped into a single 'unknown'. As a result, they have been underappreciated in terms of their contribution to the pan-Arctic lateral flux budget and their potential sensitivity to climate change as opposed to their bigger siblings. While continuing the scientific focus on large catchment

380 studies (BS) in the Arctic remains vital, we suggest to, in parallel, strongly increase focus pan-Arcticat small catchments situated entirely at high latitudes. These catchments are experiencing the greatest climatic warming while also storing large quantities of soil carbon in landscapes that are especially prone to degradation of permafrost (i.e., IWP terrain) and associated hydrological regime shifts. Using our database these and many other variables are now quantified and made spatially explicit (fig. 3, 4).

385 **4. Database availability**

Data are publicly available on https://dataverse.nl/dataset.xhtml?persistentId=doi:10.34894/U9HSPV under Creative Commons License Attribution 4.0 International (CC BY 4.0).

5. Outlook and future development

ARCADE is the first aggregated database of pan-Arctic river catchments that includes small watersheds

390 at a high resolution. The publication of this database is a necessary step toward more integrated monitoring of the pan-Arctic watershed. An important addition in the following version will be discharge data and derived seasonality (and changes therein) from the RADR database (Feng et al., 2021), which recently greatly advanced understanding of discharge in smaller arctic rivers. Another important future addition will be the delineations of subbasins and data on river biogeochemistry that is available, albeit

395   non-uniformly and largely unaggregated throughout literature. When numerous valuable datasets from various scientific disciplines are merged, it will be possible to better understand the Arctic's changing hydrology and biogeochemistry. This allows the scientific community to form new hypotheses that direct scientific efforts to specific regions and processes that may have remained under the radar.

References

Aagaard, K. and Carmack, E. C.: The role of sea ice and other fresh water in the Arctic circulation, 94, https://doi.org/10.1029/jc094ic10p14485, 1989.

405 Alvarez-Garreton, C., Mendoza, P. A., Pablo Boisier, J., Addor, N., Galleguillos, M., Zambrano-Bigiarini, M., Lara, A., Puelma, C., Cortes, G., Garreaud, R., McPhee, J., and Ayala, A.: The CAMELS-CL dataset: Catchment attributes and meteorology for large sample studies-Chile dataset, 22, https://doi.org/10.5194/hess-22-5817-2018, 2018.

AMAP: Arctic Climate Change Update 2021: Key Trends and Impacts. Summary for Policy-makers., Arctic Monitoring and Assessment Programme (AMAP), 2021.

410 Behnke, M. I., McClelland, J. W., Tank, S. E., Kellerman, A. M., Holmes, R. M., Haghipour, N., Eglinton, T. I., Raymond, P. A., Suslova, A., Zhulidov, A. V., Gurtovaya, T., Zimov, N., Zimov, S., Mutter, E. A., Amos, E., and Spencer, R. G. M.: Pan-Arctic Riverine Dissolved Organic Matter: Synchronous Molecular Stability, Shifting Sources and Subsidies, 35, https://doi.org/10.1029/2020GB006871, 2021.

Berghuijs, W. R., Woods, R. A., and Hrachowitz, M.: A precipitation shift from snow towards rain leads 415 to a decrease in streamflow, 4, https://doi.org/10.1038/nclimate2246, 2014.

Biskaborn, B. K., Smith, S. L., Noetzli, J., Matthes, H., Vieira, G., Streletskiy, D. A., Schoeneich, P., Romanovsky, V. E., Lewkowicz, A. G., Abramov, A., Allard, M., Boike, J., Cable, W. L., Christiansen, H. H., Delaloye, R., Diekmann, B., Drozdov, D., Etzelmüller, B., Grosse, G., Guglielmin, M., Ingeman-Nielsen, T., Isaksen, K., Ishikawa, M., Johansson, M., Johannsson, H., Joo, A., Kaverin, D., Kholodov, 420 A., Konstantinov, P., Kröger, T., Lambiel, C., Lanckman, J. P., Luo, D., Malkova, G., Meiklejohn, I., Moskalenko, N., Oliva, M., Phillips, M., Ramos, M., Sannel, A. B. K., Sergeev, D., Seybold, C., Skryabin, P., Vasiliev, A., Wu, Q., Yoshikawa, K., Zheleznyak, M., and Lantuit, H.: Permafrost is warming at a global scale, 10, https://doi.org/10.1038/s41467-018-08240-4, 2019.

Böhner, J. and Selige, T.: Spatial prediction of soil attributes using terrain analysis and climate 425 regionalisation, 115, 2006.

Box, J. E., Colgan, W. T., Christensen, T. R., Schmidt, N. M., Lund, M., Parmentier, F. J. W., Brown, R., Bhatt, U. S., Euskirchen, E. S., Romanovsky, V. E., Walsh, J. E., Overland, J. E., Wang, M., Corell, R. W., Meier, W. N., Wouters, B., Mernild, S., Mård, J., Pawlak, J., and Olsen, M. S.: Key indicators of Arctic climate change: 1971-2017, Environmental Research Letters, 14, https://doi.org/10.1088/1748-430 9326/aafc1b, 2019.

Brodzik, M. J., Billingsley, B., Haran, T., Raup, B., and Savoie, M. H.: Erratum: EASE-Grid 2.0: Incremental but significant improvements for earth-gridded data sets (ISPRS International Journal of

Geo-Information (2012) 1 (32-45)), ISPRS International Journal of Geo-Information, 3, https://doi.org/10.3390/ijgi3031154, 2014.

435 Bruhwiler, L., Parmentier, F. J. W., Crill, P., Leonard, M., and Palmer, P. I.: The Arctic Carbon Cycle and Its Response to Changing Climate, Current Climate Change Reports, 7, https://doi.org/10.1007/s40641-020-00169-5, 2021.

Chuvieco, E., Pettinari, M. L., Lizundia-Loiola, J., Storm, T., and Padilla Parellada, M.: ESA Fire Climate Change Initiative (Fire_cci): MODIS Fire_cci Burned Area Pixel product, version 5.1[dataset], 2018.

440 Connolly, C. T., Khosh, M. S., Burkart, G. A., Douglas, T. A., Holmes, R. M., Jacobson, A. D., Tank, S. E., and McClelland, J. W.: Watershed slope as a predictor of fluvial dissolved organic matter and nitrate concentrations across geographical space and catchment size in the Arctic, Environ. Res. Lett., 13, 104015, https://doi.org/10.1088/1748-9326/aae35d, 2018.

Conrad, O., Bechtel, B., Bock, M., Dietrich, H., Fischer, E., Gerlitz, L., Wehberg, J., Wichmann, V., and 445 Böhner, J.: System for Automated Geoscientific Analyses (SAGA) v. 2.1.4, 8, https://doi.org/10.5194/gmd-8-1991-2015, 2015.

Didan, K.: MOD13C1 MODIS/Terra Vegetation Indices 16-Day L3 Global 0.05Deg CMG V006, EOSDIS Land Processes DAAC, 2015.

ECMWF: IFS Documentation CY47R1 - Part IV: Physical Processes, 2020.

450 European Space Agency (ESA), A Copernicus DEM - Global and European Digital Elevation Model (COP-DEM) [dataset], ESA, https://doi.org/10.5270/ESA-c5d3d65, 2021.

Gorelick, N., Hancher, M., Dixon, M., Ilyushchenko, S., Thau, D., and Moore, R.: Google Earth Engine: Planetary-scale geospatial analysis for everyone, 202, https://doi.org/10.1016/j.rse.2017.06.031, 2017.

Hartmann, J., Lauerwald, R., and Moosdorf, N.: A Brief Overview of the GLObal RIver Chemistry 455 Database, GLORICH, 10, https://doi.org/10.1016/j.proeps.2014.08.005, 2014.

Holmes, R. M., Coe, M. T., Fiske, G. J., Gurtovaya, T., McClelland, J. W., Shiklomanov, A. I., Spencer, R. G. M., Tank, S. E., and Zhulidov, A. V.: Climate Change Impacts on the Hydrology and Biogeochemistry of Arctic Rivers, in: Climatic Change and Global Warming of Inland Waters: Impacts and Mitigation for Ecosystems and Societies, https://doi.org/10.1002/9781118470596.ch1, 2012a.

460 Howat, I. M., Negrete, A., and Smith, B. E.: The Greenland Ice Mapping Project (GIMP) land classification and surface elevation data sets, 8, https://doi.org/10.5194/tc-8-1509-2014, 2014.

Hugelius, G., Strauss, J., Zubrzycki, S., Harden, J. W., Schuur, E. A. G., Ping, C.-L., Schirrmeister, L., Grosse, G., Michaelson, G. J., Koven, C. D., O'Donnell, J. A., Elberling, B., Mishra, U., Camill, P., Yu, Z., Palmtag, J., and Kuhry, P.: Estimated stocks of circumpolar permafrost carbon with quantified 465 uncertainty ranges and identified data gaps, Biogeosciences, 11, 6573–6593, https://doi.org/10.5194/bg-11-6573-2014, 2014.

IPCC: The Ocean and Cryosphere in a Changing Climate, https://www.ipcc.ch/report/srocc/, 2019.

IPCC: Regional fact sheet - Polar Regions, 0, 2021.

IUSS Working Group WRB: World reference base for soil resources 2014. International soil classification 470 system for naming soils and creating legends for soil maps, https://doi.org/10.1017/S0014479706394902, 2014.

Jakobsson, M., Mayer, L. A., Bringensparr, C., Castro, C. F., Mohammad, R., Johnson, P., Ketter, T., Accettella, D., Amblas, D., An, L., Arndt, J. E., Canals, M., Casamor, J. L., Chauché, N., Coakley, B., Danielson, S., Demarte, M., Dickson, M. L., Dorschel, B., Dowdeswell, J. A., Dreutter, S., Fremand, A. 475 C., Gallant, D., Hall, J. K., Hehemann, L., Hodnesdal, H., Hong, J., Ivaldi, R., Kane, E., Klaucke, I., Krawczyk, D. W., Kristoffersen, Y., Kuipers, B. R., Millan, R., Masetti, G., Morlighem, M., Noormets, R., Prescott, M. M., Rebesco, M., Rignot, E., Semiletov, I., Tate, A. J., Travaglini, P., Velicogna, I., Weatherall, P., Weinrebe, W., Willis, J. K., Wood, M., Zarayskaya, Y., Zhang, T., Zimmermann, M., and Zinglersen, K. B.: The International Bathymetric Chart of the Arctic Ocean Version 4.0. Scientific 480 Data, 7, 1, https://doi.org/10.1038/s41597-020-0520-9, 2020.

Kargel, J. S., Leonard, G. J., Bishop, M. P., Kääb, A., and Raup, B. H.: Global Land Ice Measurements from Space, https://doi.org/10.1007/978-3-540-79818-7, 2014.

Knoben, W. J. M., Freer, J. E., Peel, M. C., Fowler, K. J. A., and Woods, R. A.: A Brief Analysis of Conceptual Model Structure Uncertainty Using 36 Models and 559 Catchments, 56, 485 https://doi.org/10.1029/2019WR025975, 2020.

Lafrenière, M. J. and Lamoureux, S. F.: Effects of changing permafrost conditions on hydrological processes and fluvial fluxes, Earth-Science Reviews, 191, https://doi.org/10.1016/j.earscirev.2019.02.018, 2019.

Liljedahl, A. K., Boike, J., Daanen, R. P., Fedorov, A. N., Frost, G. V., Grosse, G., Hinzman, L. D., Iijma, 490 Y., Jorgenson, J. C., Matveyeva, N., Necsoiu, M., Raynolds, M. K., Romanovsky, V. E., Schulla, J., Tape, K. D., Walker, D. A., Wilson, C. J., Yabuki, H., and Zona, D.: Pan-Arctic ice-wedge degradation in warming permafrost and its influence on tundra hydrology, 9, 312–318, https://doi.org/10.1038/ngeo2674, 2016.

Lindsay, J. B. and Creed, I. F.: Removal of artifact depressions from digital elevation models: Towards a
495 minimum impact approach, 19, https://doi.org/10.1002/hyp.5835, 2005.

Mann, P. J., Strauss, J., Palmtag, J., Dowdy, K., Ogneva, O., Fuchs, M., Bedington, M., Torres, R.,
Polimene, L., Overduin, P., Mollenhauer, G., Grosse, G., Rachold, V., Sobczak, W. V., Spencer, R. G.
M., and Juhls, B.: Degrading permafrost river catchments and their impact on Arctic Ocean nearshore
processes, 51, https://doi.org/10.1007/s13280-021-01666-z, 2022.

500 McClelland, J. W., Holmes, R. M., Peterson, B. J., Amon, R., Brabets, T., Cooper, L., Gibson, J., Gordeev,
V. V., Guay, C., Milburn, D., Staples, R., Raymond, P. A., Shiklomanov, I., Striegl, R., Zhulidov, A.,
Gurtovaya, T., and Zimov, S.: Development of Pan-Arctic database for river chemistry, 89,
https://doi.org/10.1029/2008EO240001, 2008.

McClelland, J. W., Holmes, R. M., Dunton, K. H., and Macdonald, R. W.: The Arctic Ocean Estuary,
505 Estuaries and Coasts, 35, https://doi.org/10.1007/s12237-010-9357-3, 2012.

Mcguire, A. D., Anderson, L. G., Christensen, T. R., Scott, D., Laodong, G., Hayes, D. J., Martin, H.,
Lorenson, T. D., Macdonald, R. W., and Nigel, R.: Sensitivity of the carbon cycle in the Arctic to climate
change, Ecological Monographs, 79, https://doi.org/10.1890/08-2025.1, 2009.

Mishra, U., Hugelius, G., Shelef, E., Yang, Y., Strauss, J., Lupachev, A., Harden, J. W., Jastrow, J. D.,
510 Ping, C. L., Riley, W. J., Schuur, E. A. G., Matamala, R., Siewert, M., Nave, L. E., Koven, C. D., Fuchs,
M., Palmtag, J., Kuhry, P., Treat, C. C., Zubrzycki, S., Hoffman, F. M., Elberling, B., Camill, P.,
Veremeeva, A., and Orr, A.: Spatial heterogeneity and environmental predictors of permafrost region soil
organic carbon stocks, 7, https://doi.org/10.1126/sciadv.aaz5236, 2021.

Moore, I. D., Gessler, P. E., Nielsen, G. A., and Peterson, G. A.: Soil Attribute Prediction Using Terrain
515 Analysis, 57, https://doi.org/10.2136/sssaj1993.03615995005700020058x, 1993.

Muñoz-Sabater, J., Dutra, E., Agustí-Panareda, A., Albergel, C., Arduini, G., Balsamo, G., Boussetta, S.,
Choulga, M., Harrigan, S., Hersbach, H., Martens, B., Miralles, D. G., Piles, M., Rodríguez-Fernández,
N. J., Zsoter, E., Buontempo, C., and Thépaut, J. N.: ERA5-Land: A state-of-the-art global reanalysis
dataset for land applications, 13, https://doi.org/10.5194/essd-13-4349-2021, 2021.

520 Neteler, M., Bowman, M. H., Landa, M., and Metz, M.: GRASS GIS: A multi-purpose open source GIS,
31, https://doi.org/10.1016/j.envsoft.2011.11.014, 2012.

Nitze, I., Grosse, G., Jones, B. M., Romanovsky, V. E., and Boike, J.: Remote sensing quantifies
widespread abundance of permafrost region disturbances across the Arctic and Subarctic, 9,
https://doi.org/10.1038/s41467-018-07663-3, 2018.

525 Obu, J., Westermann, S., Bartsch, A., Berdnikov, N., Christiansen, H. H., Dashtseren, A., Delaloye, R., Elberling, B., Etzelmüller, B., Kholodov, A., Khomutov, A., Kääb, A., Leibman, M. O., Lewkowicz, A. G., Panda, S. K., Romanovsky, V., Way, R. G., Westergaard-Nielsen, A., Wu, T., Yamkhin, J., and Zou, D.: Northern Hemisphere permafrost map based on TTOP modelling for 2000–2016 at 1 km2 scale, Earth-Science Reviews, 193, https://doi.org/10.1016/j.earscirev.2019.04.023, 2019.

530 Ono, J., Watanabe, M., Komuro, Y., Tatebe, H., and Abe, M.: Enhanced Arctic warming amplification revealed in a low-emission scenario, 3, https://doi.org/10.1038/s43247-022-00354-4, 2022.

Overland, J., Dunlea, E., Box, J. E., Corell, R., Forsius, M., Kattsov, V., Olsen, M. S., Pawlak, J., Reiersen, L. O., and Wang, M.: The urgency of Arctic change, Polar Science, 21, https://doi.org/10.1016/j.polar.2018.11.008, 2019.

535 Parmentier, F. J. W., Christensen, T. R., Rysgaard, S., Bendtsen, J., Glud, R. N., Else, B., van Huissteden, J., Sachs, T., Vonk, J. E., and Sejr, M. K.: A synthesis of the arctic terrestrial and marine carbon cycles under pressure from a dwindling cryosphere, 46, https://doi.org/10.1007/s13280-016-0872-8, 2017.

Pekel, J. F., Cottam, A., Gorelick, N., and Belward, A. S.: High-resolution mapping of global surface water and its long-term changes, 540, https://doi.org/10.1038/nature20584, 2016.

540 Poggio, L., De Sousa, L. M., Batjes, N. H., Heuvelink, G. B. M., Kempen, B., Ribeiro, E., and Rossiter, D.: SoilGrids 2.0: Producing soil information for the globe with quantified spatial uncertainty, 7, https://doi.org/10.5194/soil-7-217-2021, 2021.

Ran, Y., Li, X., Cheng, G., Che, J., Aalto, J., Karjalainen, O., Hjort, J., Luoto, M., Jin, H., Obu, J., Hori, M., Yu, Q., and Chang, X.: New high-resolution estimates of the permafrost thermal state and 545 hydrothermal conditions over the Northern Hemisphere, 14, https://doi.org/10.5194/essd-14-865-2022, 2022.

Renard, K. G., Laflen, J. M., Foster, G. R., and McCool, D. K.: The revised universal soil loss equation, in: Soil Erosion Research Methods, https://doi.org/10.1201/9780203739358, 2017.

Schuur, E. a. G., McGuire, A. D., Schädel, C., Grosse, G., Harden, J. W., Hayes, D. J., Hugelius, G., 550 Koven, C. D., Kuhry, P., Lawrence, D. M., Natali, S. M., Olefeldt, D., Romanovsky, V. E., Schaefer, K., Turetsky, M. R., Treat, C. C., and Vonk, J. E.: Climate change and the permafrost carbon feedback, 520, 171–179, https://doi.org/10.1038/nature14338, 2015.

Sen, P. K.: Estimates of the Regression Coefficient Based on Kendall's Tau, 63, https://doi.org/10.1080/01621459.1968.10480934, 1968.

555 Speetjens, N. J., Hugelius, G., Gumbricht, T., Lantuit, H., Berghuijs, W.R., Pika, P.A., Poste, A., Vonk, J.E.: ARCADE, the pan-ARctic CAtchments DatabasE, DataverseNL [data-set], https://doi.org/10.34894/U9HSPV, 2022.

Team, G.: GISS Surface Temperature Analysis (GISTEMP), version 4, 124, 2021.

Terhaar, J., Lauerwald, R., Regnier, P., Gruber, N., and Bopp, L.: Around one third of current Arctic
560 Ocean primary production sustained by rivers and coastal erosion, 12, https://doi.org/10.1038/s41467-020-20470-z, 2021.

Theobald, D. M., Harrison-Atlas, D., Monahan, W. B., and Albano, C. M.: Ecologically-relevant maps of landforms and physiographic diversity for climate adaptation planning, 10, https://doi.org/10.1371/journal.pone.0143619, 2015.

565 Vincent, W. F.: Arctic climate change: Local impacts, global consequences, and policy implications, in: The Palgrave Handbook of Arctic Policy and Politics, https://doi.org/10.1007/978-3-030-20557-7_31, 2019.

Vonk, J. E. and Gustafsson, Ö.: Permafrost-carbon complexities, Nature Geoscience, https://doi.org/10.1038/ngeo1937, 2013.

570 Walvoord, M. A. and Kurylyk, B. L.: Hydrologic Impacts of Thawing Permafrost-A Review, 15, https://doi.org/10.2136/vzj2016.01.0010, 2016.

Wild, B., Andersson, A., Bröder, L., Vonk, J., Hugelius, G., McClelland, J. W., Song, W., Raymond, P. A., and Gustafsson, Ö.: Rivers across the Siberian Arctic unearth the patterns of carbon release from thawing permafrost, 116, https://doi.org/10.1073/pnas.1811797116, 2019.

575 Yamanouchi, T. and Takata, K.: Rapid change of the Arctic climate system and its global influences - Overview of GRENE Arctic climate change research project (2011–2016), Polar Science, 25, https://doi.org/10.1016/j.polar.2020.100548, 2020.

Zanaga, D., Van De Kerchove, R., De Keersmaecker, W., Souverijns, N., Brockmann, C., Quast, R., Wevers, J., Grosu, A., Paccini, A., Vergnaud, S., Cartus, O., Santoro, M., Fritz, S., Georgieva, I., Lesiv,
580 M., Carter, S., Herold, M., Linlin, L., Tsendbazar, N., Raimoino, F., and Arino, O.: ESA WorldCover 10 m 2020 v100, 2021.

Zhang, T., Heginbottom, J. A., Barry, R. G., and Brown, J.: Further statistics on the distribution of permafrost and ground ice in the Northern Hemisphere, 24, https://doi.org/10.1080/10889370009377692, 2000.

585 Zhang, T., Barry, R. G., Knowles, K., Heginbottom, J. A., and Brown, J.: Statistics and characteristics of permafrost and ground-ice distribution in the Northern Hemisphere, 31, https://doi.org/10.1080/10889370802175895, 2008.

Table 1 Summary statistics of the pan-Arctic watersheds database focused on permafrost. Note that this summary excludes watersheds that are fully covered by glaciers/icesheets.

Group*	count	Total area (km²)	% of total area	Mean elevation (m amsl*)	Mean slope (°)	Permafrost Continuous	Permafrost Discontinuous	Permafrost Sporadic	Ice-wedge terrain	Mean ALT* (cm)	MAAT* (°C)
BS	7	1.31×10⁷	50%	289	2.5	19% ±26.8%	19% ±13.6%	14% ±11.2%	1%	126 ±29	-2.9 ±3.7
MN	9	2.31×10⁶	12%	306	2.0	57% ±46.8%	11% ±17.1%	8% ±14.1%	10%	94 ±14	-10.5 ±7.6
PAT	929	6.09×10⁶	29%	212	1.6	48% ±46.1%	12% ±28.5%	9% ±23.5%	31%	98 ±42	-10.4 ±6.1
PAS	45124	2.23×10⁶	9%	112	3.4	57% ±46.4%	9% ±26.5%	7% ±21.9%	37%	93 ±45	-9.1 ±5.8
Total	46069	2.37×10⁷	100%	230	2.4	45% ±84.8%	13% ±44.6%	9% ±36.8%	20%	103 ±32	-8.2 ±5.8

*Abbreviations stand for the grouped watersheds by area, Big Seven (BS), Middle Nine (MN), Pan-Arctic Thousands (PAT), Pan-Arctic Small watersheds (PAS); count represents the number of catchments covered by the subsequent data columns; amsl stands for 'above mean sea level'; ALT stands for 'Active Layer Thickness'; MAAT stands for 'Mean Annual Air Temperature'.

590

Table 2 Watershed topographic properties summarized by group (classification based on area) and relevant (sub)continent.

Group*	Continent	count	Max. mean slope (°)	Mean slope (°)	Mean area (km²)	Total area (km²)	Mean elevation (m)	Water (%)	Ice (%)	Mean TWI*	Mean LS*
BS	Eurasia	4	4.9	3.1 ±1.54	2283485	9133939	290 ±103.1	2%	0%	6.6 ±1.29	3.1 ±1.57
BS	North America	3	3.7	2.5 ±1.53	1313306	3939919	290 ±64.3	7%	0%	6.8 ±2.25	2.7 ±1.93
MN	Eurasia	8	4.7	1.8 ±1.59	259073	2072580	154 ±122.2	3%	0%	6.9 ±1.90	1.7 ±1.86
MN	North America	1	0.6	0.6 ±0.00	238539	238539	135 ±0.0	22%	0%	8.7 ±0.00	0.2 ±0.00
PAT	Eurasia	285	8.8	1.6 ±1.71	6444	1836498	97 ±115.8	7%	1%	6.9 ±1.95	1.5 ±2.39
PAT	Greenland	140	10.7	2.3 ±2.42	4781	669384	532 ±259.2	1%	77%	4.8 ±1.45	3.2 ±3.97
PAT	North America	504	9.9	1.5 ±1.72	7105	3581003	133 ±127.0	10%	5%	6.2 ±1.76	1.4 ±2.26
PAS	Eurasia	14269	27.0	3.1 ±4.10	45	645781	80 ±108.2	6%	6%	5.6 ±1.88	3.9 ±6.64
PAS	Greenland	7848	28.9	7.5 ±5.04	40	310800	258 ±179.8	2%	29%	3.7 ±0.98	11.7 ±9.88
PAS	North America	22996	23.1	2.4 ±2.99	55	1272918	81 ±112.3	8%	4%	5.2 ±1.58	2.7 ±4.90
Total	Pan-Arctic	46058	12.2	2.6 ±8.37	411287	23701361	205 ±427.8	7%	12%	6.1 ±5.13	3.2 ±14.21

* **Abbreviations stand for the grouped watersheds by area, Big Seven (BS), Middle Nine (MN), Pan-Arctic Thousands (PAT), Pan-Arctic Small watersheds (PAS); count represents the number of catchments covered by the subsequent data columns**; TWI stands for 'Topographic Wetness Index' and is based on the SAGA Wetness Index Tool; LS stands for 'Slope Steepness and Length Factor'.

Table 3 Watershed permafrost properties summarized by group (based on area) and relevant (sub)continent.

Group*	Continent	count	Continuous permafrost	Discontinuous permafrost	Sporadic permafrost	IWP* terrain	OCS$_{0-30cm}$ (t ha^{-1})	ALT* mean (cm)
BS	Eurasia	4	30% ±31.8%	18% ±12.5%	10% ±6.7%	2 ±4.3%	67 ±3.7	128 ±29.3
BS	North America	3	4% ±4.6%	20% ±17.9%	20% ±15.0%	3 ±2.2%	62 ±4.7	118 ±29.9
MN	Eurasia	8	59% ±49.6%	7% ±11.6%	8% ±15.1%	10 ±12.1%	78 ±14.5	87 ±12.4
MN	North America	1	40% ±0.0%	46% ±0.0%	7% ±0.0%	39 ±0.0%	61 ±0.0	112 ±0.0
PAT	Eurasia	285	43% ±47.5%	18% ±35.2%	10% ±25.4%	40 ±39.9%	83 ±12.9	96 ±56.9
PAT	Greenland	140	15% ±24.7%	2% ±6.8%	0% ±1.7%	4 ±8.5%	92 ±13.9	105 ±49.3
PAT	North America	504	59% ±45.3%	12% ±27.1%	11% ±25.0%	37 ±38.1%	71 ±11.2	96 ±28.0
PAS	Eurasia	14279	41% ±46.7%	11% ±29.4%	6% ±20.9%	38 ±42.9%	88 ±13.1	89 ±55.4
PAS	Greenland	7848	35% ±41.4%	11% ±26.2%	7% ±21.2%	13 ±28.2%	87 ±14.4	113 ±63.4
PAS	North America	22996	74% ±40.8%	8% ±24.6%	7% ±22.7%	45 ±43.9%	71 ±12.3	87 ±24.7
Total	Pan-Arctic	46068	40% ±118.2%	15% ±69.2%	9% ±56.3%	23% ±88.6%	76 ±35.5	103 ±126.7

***Abbreviations stand for the grouped watersheds by area, Big Seven (BS), Middle Nine (MN), Pan-Arctic Thousands (PAT), Pan-Arctic Small watersheds (PAS); count represents the number of catchments covered by the subsequent data columns**; IWP stands for 'Ice Wedge Polygon'; OCS$_{0-30cm}$ stands for "Organic Carbon Stock in the upper 0-30 cm of the soil; ALT stands for 'Active Layer Thickness'.

Table 4 Watershed land-cover type and properties summarized by group (classification based on area) and relevant (sub)continent.

Group*	Continent	count	Trees	Shrub	Grassland	Cropland	Built-up	Barren	Snow/ice	Water	Wetland
BS	Eurasia	4	56 ±19.2%	1 ±0.9%	24 ±10.1%	3.6 ±6.53%	0.1 ±0.11%	2 ±1.2%	0 ±0.0%	3 ±0.7%	4 ±3.9%
BS	North America	3	47 ±9.1%	5 ±0.6%	23 ±7.6%	9.0 ±14.61%	0.1 ±0.16%	2 ±1.1%	1 ±1.0%	8 ±4.9%	1 ±0.5%
MN	Eurasia	8	53 ±26.6%	0 ±0.2%	23 ±17.3%	0.1 ±0.33%	0.0 ±0.03%	1 ±1.5%	0 ±0.0%	4 ±2.8%	8 ±8.2%
MN	North America	1	6 ±0.0%	0 ±0.0%	51 ±0.0%	0.0 ±0.00%	0.0 ±0.00%	1 ±0.0%	0 ±0.0%	26 ±0.0%	1 ±0.0%
PAT	Eurasia	285	12 ±22.2%	0 ±0.4%	36 ±20.8%	0.1 ±0.32%	0.0 ±0.08%	4 ±8.7%	2 ±7.7%	8 ±7.4%	21 ±22.8%
PAT	Greenland	140	0 ±0.1%	0 ±0.0%	4 ±7.6%	0.0 ±0.00%	0.0 ±0.00%	8 ±10.1%	77 ±27.8%	2 ±2.8%	0 ±0.1%
PAT	North America	504	8 ±17.3%	3 ±8.4%	25 ±24.0%	0.0 ±0.02%	0.0 ±0.01%	12 ±14.4%	5 ±17.3%	12 ±9.5%	5 ±10.4%
PAS	Eurasia	14279	10 ±21.8%	0 ±0.5%	29 ±30.4%	0.2 ±1.88%	0.1 ±1.34%	10 ±21.3%	6 ±18.1%	7 ±11.1%	27 ±33.2%
PAS	Greenland	7848	0 ±0.5%	0 ±0.0%	14 ±22.3%	0.0 ±0.00%	0.0 ±0.36%	23 ±22.0%	30 ±33.6%	5 ±7.8%	1 ±3.8%
PAS	North America	22997	2 ±10.9%	1 ±5.6%	16 ±23.2%	0.0 ±0.05%	0.0 ±0.13%	30 ±28.3%	5 ±16.7%	10 ±11.7%	14 ±22.8%
Total	Pan-Arctic	46069	19% ±50.4%	1% ±10.1%	25% ±59.0%	1% ±16.1%	0% ±1.4%	9% ±46.1%	13% ±53.6%	8% ±22.5%	8% ±48.5%

615 *Abbreviations stand for the grouped watersheds by area, Big Seven (BS), Middle Nine (MN), Pan-Arctic Thousands (PAT), Pan-Arctic Small watersheds (PAS); count represents the number of catchments covered by the subsequent data columns

620 **Table 5 Watershed climatological properties summarized by group (classification based on area) and relevant (sub)continent.**

Group*	Continent	count	T min. (°C)	T max. (°C)	T mean (°C)	ΔT mean (°C 30y⁻¹)	ET mean (mm yr⁻¹)	P mean (mm yr⁻¹)	ΔP mean (mm yr⁻¹)	Q mean (mm yr⁻¹)	max. Snow depth (m)	max. Snowmelt (mm d⁻¹)
BS	Eurasia	4	-20.0 ±4.38	9.0 ±4.69	-5.5 ±4.95	1.7 ±0.65	325 ±74.4	513 ±66.3	1.2 ±1.60	193 ±30.9	0.7 ±0.08	4.0 ±0.37
BS	North America	3	-16.3 ±3.02	12.2 ±4.13	-2.1 ±3.38	1.5 ±0.96	377 ±112.0	541 ±50.7	1.1 ±1.79	178 ±53.6	0.7 ±0.35	3.3 ±0.97
MN	Eurasia	8	-22.3 ±5.19	5.7 ±4.93	-8.3 ±5.62	2.8 ±0.88	243 ±73.9	515 ±150.4	1.0 ±1.30	274 ±108.2	0.7 ±0.19	4.9 ±1.84
MN	North America	1	-21.8 ±0.00	5.8 ±0.00	-9.0 ±0.00	1.8 ±0.00	255 ±0.0	421 ±0.0	0.3 ±0.00	170 ±0.0	0.6 ±0.00	3.4 ±0.00
PAT	Eurasia	285	-18.3 ±6.28	5.8 ±4.77	-6.4 ±5.97	3.4 ±1.42	192 ±69.9	601 ±376.6	3.7 ±3.50	403 ±350.4	1.6 ±3.94	6.1 ±3.04
PAT	Greenland	140	-26.0 ±4.08	-4.8 ±4.33	-15.5 ±4.25	2.0 ±0.38	24 ±37.8	561 ±454.1	1.8 ±7.77	67 ±123.5	29.6 ±7.81	1.0 ±1.63
PAT	North America	504	-21.8 ±4.44	3.1 ±6.37	-10.0 ±5.18	2.5 ±0.75	200 ±99.3	462 ±229.0	1.8 ±3.46	257 ±183.2	2.9 ±6.89	4.6 ±2.14
PAS	Eurasia	14272	-13.8 ±7.89	4.7 ±5.77	-4.7 ±6.88	3.4 ±1.79	199 ±149.7	794 ±591.9	3.6 ±5.29	564 ±530.3	5.7 ±10.85	6.3 ±3.57
PAS	Greenland	7844	-18.3 ±5.33	0.8 ±5.35	-9.0 ±5.26	2.3 ±0.56	65 ±76.1	790 ±578.0	2.9 ±12.70	334 ±359.8	20.1 ±14.70	4.5 ±4.40
PAS	North America	22989	-20.6 ±4.76	-0.2 ±5.22	-11.0 ±4.54	2.5 ±0.83	160 ±86.4	401 ±204.1	1.6 ±3.37	225 ±169.5	4.0 ±8.67	4.5 ±2.09
Total	Pan-Arctic	46050	-19.9 ±15.63	4.2 ±15.31	-8.2 ±15.61	2.4 ±3.01	204 ±274.6	560 ±1075.2	1.9 ±17.11	266 ±791.5	6.7 ±23.09	4.3 ±7.58

*Abbreviations stand for the grouped watersheds by area, Big Seven (BS), Middle Nine (MN), Pan-Arctic Thousands (PAT), Pan-Arctic Small watersheds (PAS); count represents the number of catchments covered by the subsequent data columns; T stands for temperature, ET stands for total evapotranspiration, P stands for precipitation and Q stands for 625 runoff. ΔT mean and ΔP mean are calculated from the Sen slope of the monthly mean Temperature and Precipitation over the period 1999 – 2019 (mo⁻¹) multiplied by the number of months.
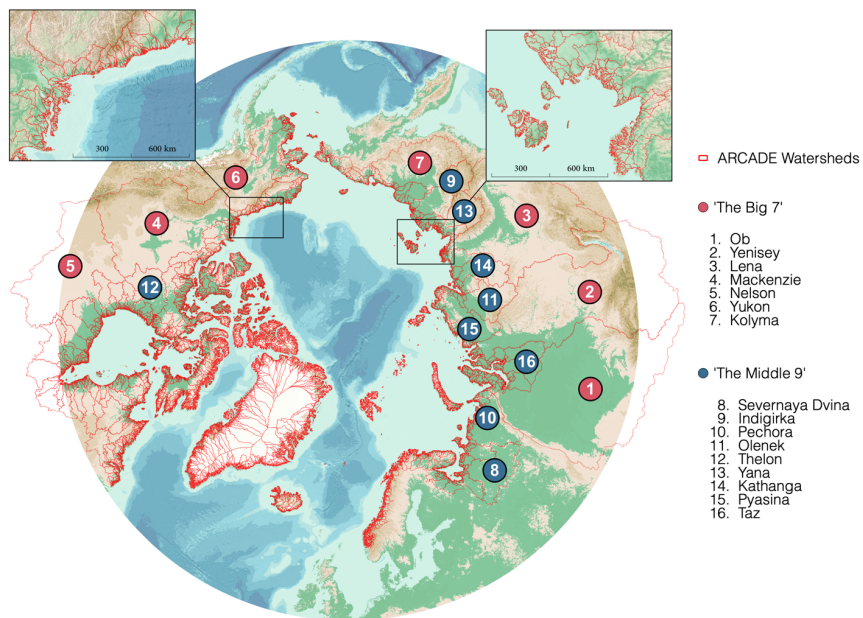
Figure 1. Circumpolar map of all ARCADE watersheds, 1 km² and larger, Strahler order 5 and higher, at 90-meter resolution with insets of the Southern Beaufort Sea region (upper left) and the Laptev Sea coast, including the New Siberian Islands (upper right). (Background map: International Bathymetric Chart of the Arctic Ocean V4.0 (IBCAO) (Jakobsson et al., 2020)).

635
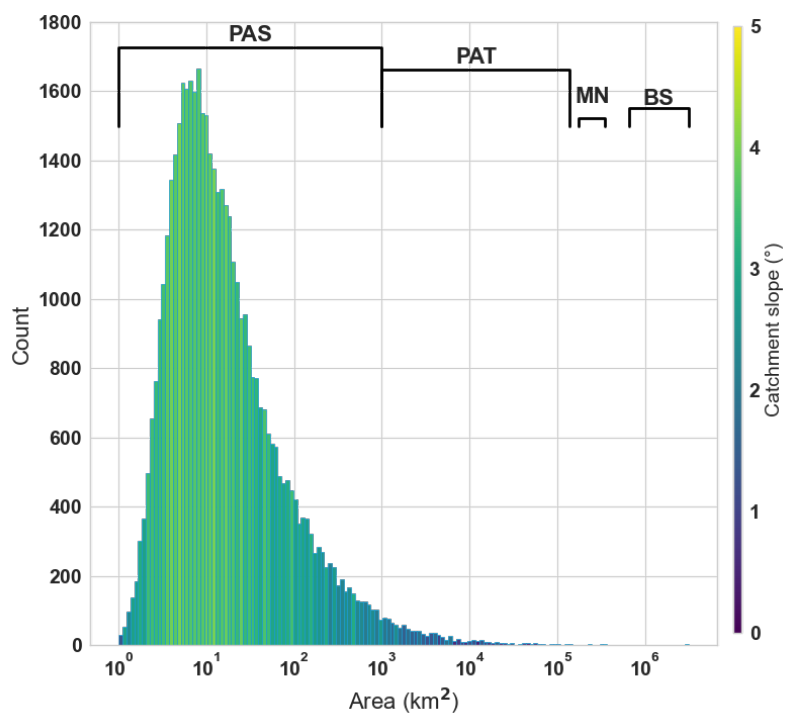
Figure 2. The distribution of watershed areas in the pan-Arctic watersheds database and the range of the four groups that classify based on watershed area. 'BS' stands for 'Big Seven', 'MN' for 'Middle Nine', 'PAT' for 'Pan-Arctic Thousands', and PAS for 'Pan-Arctic Small watersheds. Note that the x-axis has a logarithmic scale. The color of the bars represents the mean bin catchment slope of the.

640

645

650
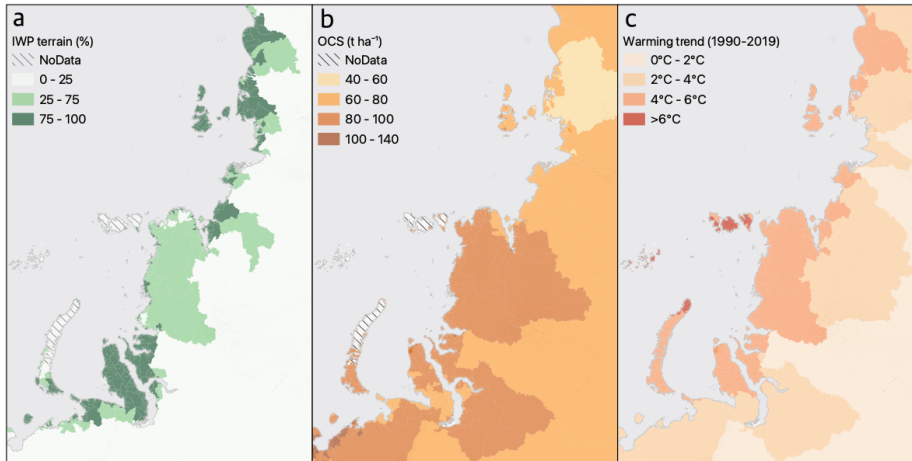
Figure 3. Siberian coastal watersheds with Ice wedge polygon (IWP) terrain (% watershed coverage) (a), soil organic carbon stock (OCS) in metric tons per hectare (b), and the mean watershed temperature trend taken over the period 1990 – 2019 (c) (map source: ARCADE database (Speetjens et al., 2022)).
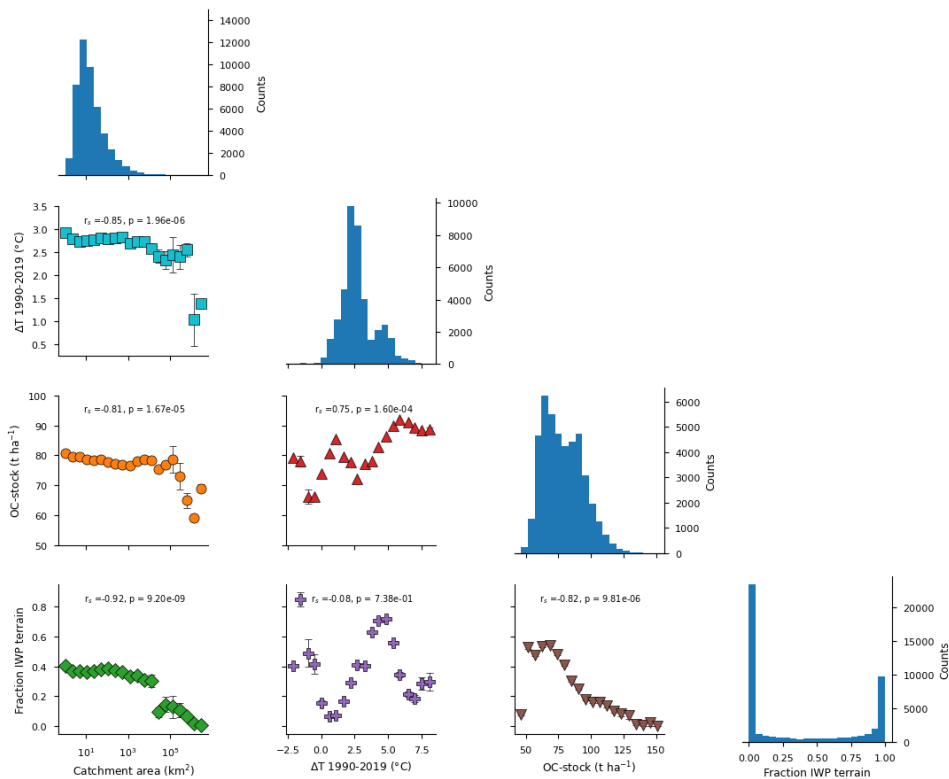
Figure 4. Correlations of binned data of selected catchment properties from our database. We calculated Spearman's Rho on the binned data. Most notably, we observe that small watersheds have experienced the greatest warming, while having the highest mean carbon stocks and the highest fraction of IWP terrain. Similarly, the data show that high OC stocks are found where most warming has occurred.

660